THE JOURNAL OF PHYSICAL CHEMISTRY A

Article

pubs.acs.org/JPCA

Size Matters in the Water Uptake and Hygroscopic Growth of Atmospherically Relevant Multicomponent Aerosol Particles

Olga Laskina,[†] Holly S. Morris,[†] Joshua R. Grandquist,[‡] Zhen Qin,[†] Elizabeth A. Stone,[†] Alexei V. Tivanski,*[,†] and Vicki H. Grassian*[,†,‡]

[†]Department of Chemistry, and [‡]Department of Chemical and Biochemical Engineering, University of Iowa, Iowa City, Iowa 52242, United States

Supporting Information

ABSTRACT: Understanding the interactions of water with atmospheric aerosols is crucial for determining the size, physical state, reactivity, and climate impacts of this important component of the Earth's atmosphere. Here we show that water uptake and hygroscopic growth of multicomponent, atmospherically relevant particles can be size dependent when comparing 100 nm versus ca. 6 μm sized particles. It was determined that particles composed of ammonium sulfate with succinic acid and of a mixture of chlorides typical of the marine environment show size-dependent hygroscopic behavior. Microscopic analysis of the distribution of components within the aerosol particles show that the size dependence is due to differences in the mixing state, that is, whether particles are homogeneously mixed or phase separated, for different sized particles. This morphology-dependent hygroscopicity has consequences for heterogeneous atmospheric chemistry as well as aerosol interactions with electromagnetic radiation and clouds.

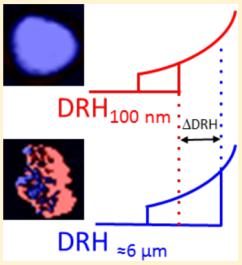

INTRODUCTION

The hygroscopic behavior and cloud condensation nuclei activity of multicomponent atmospheric aerosol particles depend on the mixing state of the particles.[1,2] It has been previously shown that when organic compounds are mixed with inorganic salts, both the deliquescence relative humidity and efflorescence relative humidity, DRH and ERH, respectively, of the salt decrease when these components are homogeneously mixed.[3] As a result of the lowering of both the DRH and ERH, these particles remain in the liquid state over the relative humidity (RH) range typically experienced by particles in the atmosphere. In contrast, when the organic component phase separates from the inorganic salt, there is little or no change in DRH and ERH values from those of the pure salt.[3−8] Although these differences in the water uptake and hygroscopic growth between homogeneously mixed and phase separated aerosol particles are well understood, what is not clear is whether hygroscopic properties and mixing states can depend on particle size.

In general phase separation in particles depends on composition, including organic material, inorganic salt, and organic-to-inorganic ratio.[3−8] Previously, it was inferred that phase separation behavior for ammonium sulfate (AS) when mixed with secondary organic material is size-independent.[8] However, Veghte et al. recently reported size-dependent liquid−liquid phase separation for organic−inorganic mixtures of ammonium sulfate mixed with pimelic acid.[9] Liquid−liquid phase separation in larger particles leads to phase separation in these particles upon lowering the RH, whereas smaller particles are homogeneous at all RH. Thus, the size of particles can result in different mixing states and therefore may yield to different hygroscopic properties. Since the mixing state, whether components are homogeneously mixed or phase separated, for multicomponent aerosol particles can be size dependent, we hypothesize that this will also lead to size-dependent water uptake properties in multicomponent aerosol particles. The determination of size-dependent hygroscopic growth due to differences in mixing state in the size is essential to better understanding aerosol reactivity and climate forcing.

Typically, water uptake and hygroscopic growth of submicrometer aerosol particles are studied by hygroscopic tandem differential mobility analyzers (HTDMA), whereas supermicrometer particles are often studied by microscopy methods such as micro-Raman or infrared spectroscopy, for which particles are typically substrate-deposited for these optical measurements, along with substrate-free methods such as particle levitation techniques.[7,10−16] In this study, we investigate the size-dependent mixing state, water uptake, and hygroscopic properties of multicomponent aerosol particles using HTDMA and micro-Raman spectroscopy. Mixtures of sodium, magnesium, calcium, and potassium chlorides were studied as the most abundant inorganic components of sea spray aerosol.[17] Additionally, a mixture of AS with succinic acid (SA), representative of mixed inorganic−organic aerosols, was studied.[18] To understand the mixing states of these mixtures, we utilized several complementary microscopy techniques including atomic force microscopy (AFM), scanning electron microscopy coupled with energy dispersive X-ray spectroscopy

Special Issue: A: Mario Molina Festschrift

Received: October 11, 2014
Revised: November 25, 2014
Published: December 17, 2014

DOI: 10.1021/jp510268p
J. Phys. Chem. A 2015, 119, 4489−4497

(SEM/EDX), and chemical functional group mapping using micro-Raman spectroscopy. As discussed and shown here for the first time, the size dependence of water uptake and hygroscopic growth is a result of the aerosol particle mixing state.

EXPERIMENTAL SECTION

Sample Preparation. Aerosol particles are formed by atomizing (TSI Inc., model 3076) solutions in Optima water (Fisher Scientific). Ammonium sulfate (NH_4SO_4, AS), sodium chloride (NaCl), and potassium chloride (KCl) are purchased from Fisher Scientific (all ≥99.0%); succinic acid (HOOC−$(CH_2)_2$−COOH, SA), magnesium chloride hexahydrate ($MgCl_2{\cdot}6H_2O$) and calcium chloride dihydrate ($CaCl_2{\cdot}2H_2O$) are purchased from Sigma-Aldrich (all ≥99.0%); malonic (HOOC−CH_2−COOH, MA) and adipic acids (HOOC-$(CH_2)_4$-COOH, AA) are purchased from Alfa Aesar (both 99.0%) and are used without further purification.

Pure AS and NaCl particles are prepared by atomizing solutions containing 0.5 wt % of either salt. Mixed AS/SA and AS/AA particles are prepared from solution containing 0.5 wt % AS and 0.5 wt % organic acid. That corresponds to the expected organic to inorganic mass ratio of atmospheric aerosol particles that ranges from 0.2 to 3.5.[19−21] Mixed NaCl/MA particles are prepared from a solution containing 0.5 wt % NaCl and 2:1 molar ratio between NaCl and MA. A mixture of chlorides is prepared from solution of NaCl, $MgCl_2{\cdot}6H_2O$, $CaCl_2{\cdot}2H_2O$, and KCl with a ratio of Na^+, Mg^{2+}, Ca^{2+}, K^+ = 1:0.11:0.02:0.02 wt %, respectively, to mimic the composition of seawater[17] and therefore is referred to as a marine chloride mixture. Upon exiting the atomizer, aerosols with a flow rate of 1.5 Lpm are passed through a diffusion dryer (TSI Inc., model 3062) to reduce the relative humidity (RH) to <5%.

Hygroscopic Tandem Differential Mobility Analyzer (HTDMA). Hygroscopicity as a function of increasing and decreasing RH of 100 nm particles at 298 K is measured using a HTDMA system. For these measurements, dehydrated aerosol particles are size-selected at 100 nm with a differential mobility analyzer (DMA; TSI, Inc. model 3080). The monodispersed aerosols are directed to a hydration chamber that was equilibrated at different RH values. The RH is adjusted by varying the ratio of wet and dry air supplied by a commercial dry air generator (Parker Balston, model 75-62). A portion of the dry air is sent through a bubbler to humidify. The dried aerosol and humidified air are combined in the hydration chamber. Then the aerosol particles are directed to a scanning mobility particle sizer (SMPS; TSI, Inc., model 3936) that consists of a DMA (TSI, Inc., model 3080) and a condensation particle counter (CPC; TSI, Inc., model 3025A) where the size distributions of the humidified aerosol are measured. Hygroscopicity curves are obtained by measuring the change in particle diameter with increasing and decreasing RH. RH is changed stepwise and size distribution is measured as soon as RH stabilizes after being changed (5−20 min). RH steps are 5−7% in the RH range in which no phase transitions are expected and 0.1−0.5% in the RH range close to expected DRH and ERH. Size distribution data are fit to a Gaussian curve to obtain particle diameters. At each RH value, the total hygroscopic growth is expressed as the growth factor, g(RH) calculated according to eq 1:

$$g(\mathrm{RH}) = \frac{D_p(\mathrm{RH})}{D_o} \quad (1)$$

where D_p(RH) is a particle diameter at a particular RH value and D_0 is the diameter of the dry particle. Growth factor is then plotted as a function of RH.

Micro-Raman Spectroscopy. Supermicron-sized aerosol particles (3−12 μm) were collected for 3 to 5 min by placing hydrophobically coated quartz substrates (Ted Pella Inc., part no. 16001-1) on the surface of the impactor installed in front of the DMA (which is normally used to remove particles larger than 1 μm). The hydrophobic coating was prepared by dipping the substrate into a beaker containing Rain-X,[22] a commercially available product that contains polysiloxanes. Therefore, this placement is suitable for the collection of supermicrometer-sized particles. This quartz disc is then placed inside a flow cell (Linkam microscope stage LTS120) that is situated on the motorized stage under the Raman microscope. The flow cell has an inlet and outlet valve to enable the system to be operated under a continuous stream of humidified air with the RH controlled by adjusting the ratio of wet and dry air prior to entering the stage. This design is similar to the RH control system used for HTDMA experiments described above. The flow cell with the sample inside is then placed on a motorized microscope stage. Raman spectroscopy is performed using a LabRam HR Evolution Raman spectrometer (Horiba). The spectrometer is equipped with an Olympus BX41 optical microscope. In the experiments described here, the long working distance (7.6 mm) objective lens with 100× magnification is used. Raman scattering is performed using a laser operating at 532 nm. Raman spectra is recorded in the spectral range from 100 to 4000 cm^{-1}, three exposures of 15 s each are averaged to obtain the resulting spectrum.

$$g(RH) = \frac{A_{RH}}{A_{RHo}} \quad (2)$$

where A_{RH} is integrated area of OH stretching mode of water (3050−3700 cm^{-1}) at each RH and A_{RHo} is that of a dry particle.

Raman growth factor is defined as the ratio of integrated area of OH stretching mode of water (3050−3700 cm^{-1})[23] at each RH (A_{RH}) normalized to that of a dry particle (A_{RH0}). For particles containing AS, the 3350−3700 cm^{-1} wavenumber range is used to avoid any overlap with the N−H stretching region for the ammonium ion in AS.[24] Hygroscopic growth curves are obtained by plotting the Raman growth factor as a function of RH. Similar to HTDMA experiments, the RH is changed stepwise. At each RH, a Raman spectrum is collected after the RH stabilizes (ca. several minutes). Raman maps of individual particles are collected by raster-scanning the laser focal spot and gathering point-by-point spectral data with a step size of 400 nm. The AS map is obtained by mapping the intensity of the 960−990 cm^{-1} spectral region. For SA and AA maps, the intensity of the 920−950 cm^{-1} and 900−930 cm^{-1} spectral regions is used, respectively.

Atomic Force Microscopy (AFM). For AFM imaging, aerosol particles are collected on silicon wafers (Ted Pella Inc., part no. 16008). Supermicrometer particles are collected for 3−5 min by placing a silicon wafer in the place of impaction surface of the DMA impactor as described above. Small particles are collected after being selected by DMA at 100 nm for 30 min by directing monodisperse particle flow on the

DOI: 10.1021/jp510268p
J. Phys. Chem. A 2015, 119, 4489−4497

substrate. AFM images are obtained using molecular force probe 3D AFM (Asylum Research, Santa Barbara, CA). Phase images are collected using intermittent contact mode (AC mode) and silicon probes (MikroMasch, Model CSC37) with a nominal spring constant of 0.35 N/m and a typical tip radius of curvature of 10 nm. A phase shift in the image is a result of a lag between the excitation oscillation of the cantilever and the output oscillation associated with the tip interacting with the sample surface. Viscosity, chemical composition, adhesion force, and elasticity of the sample are among factors that can cause changes in the phase.[25,26] Phase imaging therefore allows compositional contrast of heterogeneous surfaces and can reveal spatially resolved information on the sample surface that reflects differences in the physical state and/or chemical composition associated with a phase separated particle. All images are collected at room temperature and at controlled RH. Samples are placed in a humidity cell described elsewhere[25] and the RH is adjusted to below 10% and allowed to equilibrate for 5−10 min. Low RH improves phase imaging and prevents phase differences around particles due to the surrounding water layer.

Ambient Pressure Scanning Electron Microscopy Coupled with Energy Dispersive X-ray Spectroscopy (SEM/EDX). For ambient pressure SEM/EDX mapping, aerosol particles are collected upon exiting the dryers for 3−5 min on WETSEM capsules (Quantomix, part no. QX-102) avoid particles drying out completely under the vacuum environment of the SEM chamber. SEM images and maps are collected using a Hitachi S-4800 SEM. The SEM is coupled with an EDX detector equipped with iridium ultra-micro-analysis software (IXRF Systems, Inc.) for elemental analysis. The electron microscope is operated at 20 kV accelerating voltage, 10 μA current; images are collected at 8 mm working distance.

RESULTS

Ammonium Sulfate and Sodium Chloride. Raman spectra of AS and NaCl collected at low (3−4%) RH and high (85−89%) RH are shown in Figure 1 with quartz spectra

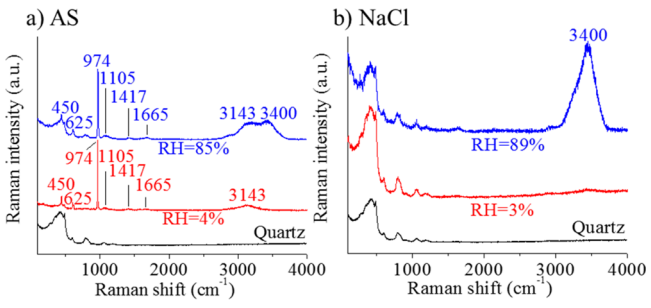

Figure 1. (a) AS and (b) NaCl Raman spectra of dry (red) and deliquesced (blue) particles are shown as representative spectra. Raman spectrum of the substrate (quartz) is also shown for reference (black).

(substrate) as a reference. As expected, dry NaCl has no vibrational transitions in the 100−4000 cm^{-1} range. Dry AS Raman spectra show SO_4^{2-} vibrational modes at 450, 625, 974, and 1105 cm^{-1} as well as NH_4^+ vibrational modes at 1417, 1665, and 3143 cm^{-1}.[24] At RH above the deliquescence point a broad band at 3400 cm^{-1} appears for both samples and originates from the O−H stretching modes of water.[23]

AS and NaCl hygroscopicity were measured using HTDMA for 100 nm particles and using micro-Raman spectroscopy for substrate-deposited supermicrometer particles. Measured hygroscopicity curves are shown in Figure 2. The DRH of AS

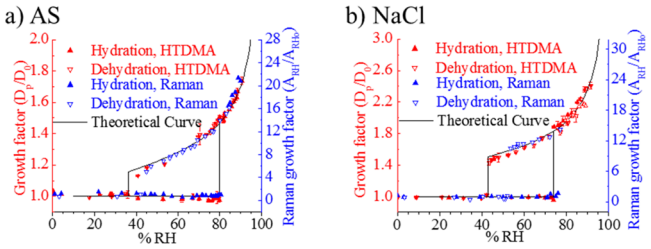

Figure 2. (a) AS and (b) NaCl hygroscopicity measured by HTDMA for 100 nm particles (red triangles) and micro-Raman results for supermicrometer particles (blue triangles). Theoretical Kohler curves are shown in black.

was determined to be 80.4 ± 0.6% RH using HTDMA and 82.3 ± 2.5% RH using micro-Raman spectroscopy. The uncertainty in DRH and ERH values for HTDMA are standard deviations of multiple (three to five) measurements. Micro-Raman spectroscopy has been performed on several individual particles (three to six), and therefore the uncertainty in DRH and ERH values are standard deviations in these values of several individual particles. These values agree well between each other and with literature values which range from 77 to 83% RH.[10,27−29] ERH was measured at 37.7 ± 4.1% RH for HTDMA and 43.5 ± 2.1% RH using micro-Raman spectroscopy. These values also agree with the range of values in the literature between 33 to 48% RH.[28−31] In general, there are larger differences in ERH values because ERH is often a kinetically controlled process, whereas the DRH is controlled by thermodynamics.[32] Therefore, it has been observed that a variety of effects and different conditions (drying rate, the presence of the substrate, particle size) may impact ERH but these do not influence DRH.

DRH values for NaCl were 74.0 ± 0.2% RH and 77.5 ± 2.1% RH as probed by HTDMA and micro-Raman spectroscopy, respectively. These values agree well with reported literature values of 74 to 76% RH within experimental error.[10,27,29,33,34] ERH values were 43.0 ± 1.0% RH and 52.8 ± 1.1% RH as probed by HTDMA and micro-Raman spectroscopy, respectively. These also are close to reported literature values of 44 to 50% RH.[34,35] DRH and ERH values for these experiments of simple single component systems (AS and NaCl) at two different sizes (i.e., submicrometer and supermicrometer) are listed in Table 1.

The growth of aqueous solution droplets in humid air can be described by the Kohler theory.[10,36,37] The diameter of the aqueous solution droplet is related to RH according to eq 3:[10]

$$\%\mathrm{RH} = a_w \exp\left(\frac{4M_w\sigma_{sol}}{RT\rho_w D_p}\right)100 \quad (3)$$

where a_w is the water activity, M_w is the molar mass of water (kg·mol^{-1}), σ_{sol} is the surface tension of solution (N·m^{-1}), ρ_w is the density of water (kg·m^{-3}), R is the ideal gas constant (J·mol^{-1}·K^{-1}), and T is the temperature (K).

A theoretical growth factor can be calculated using eq 4:[10]

DOI: 10.1021/jp510268p
J. Phys. Chem. A 2015, 119, 4489−4497

Table 1. Measured DRH and ERH Values for Single Component and Multicomponents Particle Compositions at Two Size Ranges: 100 nm, Submicron, As Measured Using the HTDMA System, and 3−10 μm, Supermicron, As Measured Using Micro-Raman Spectroscopy

	DRH (% RH)		ERH (% RH)	
sample mixture	submicrometer	supermicrometer	submicrometer	supermicrometer
pure AS	80.4 ± 0.6	82.3 ± 2.5	37.7 ± 4.1	43.5 ± 2.1
pure NaCl	74.0 ± 0.2	77.5 ± 2.1	43.0 ± 1.0	52.8 ± 1.1
NaCl/MA (2/1 molar)	67.0 ± 4.4	71.8 ± 5.3	36.2 ± 0.4	49.1 ± 1.6
AS/AA (1:1 wt %)	79.3 ± 0.5	82.2 ± 0.6	31.8 ± 1.7	44.6 ± 1.3
AS/SA (1:1 wt %)	73.2 ± 0.6	82.7 ± 0.3	29.2 ± 6.1	45.5 ± 1.1
marine chloride mixture	66.1 ± 0.1	75.3 ± 1.1	40.0 ± 1.2	49.0 ± 0.7

AS= ammonium sulfate; MA = malonic acid; AA = adipic acid; SA = succinic acid.

$$g(\mathrm{RH}) = \left(\frac{\rho_s}{\frac{c_{sol}}{100}\rho_{sol}} \right)^{1/3} \quad (4)$$

where ρ_s is the solute density (kg·m^{-3}), ρ_{sol} is the solution density (kg·m^{-3}), and c_{sol} is the solution concentration (mass percent). Theoretical growth curve can therefore be calculated by combining eqs 1, 3−4 as described in Gibson et al.[38]

Hygroscopic growth curves for NaCl and AS were calculated using Kohler theory and are shown in Figure 2 (black lines). Overall, as expected, the determined hygroscopicity shows that hygroscopicity curves of AS and NaCl measured by HTDMA and Raman overlap with each other and with corresponding theoretical Kohler curves. DRH and ERH values agree well with each other as well as with literature values. HTDMA and micro-Raman spectroscopy show similar and reliable results for RH values of phase transitions of sub- and supermicrometer aerosol particles, respectively. On the basis of these results it can be concluded that both HTDMA and micro-Raman methods can be used to study hygroscopicity. It should be noted here that it is preferable to use a hydrophobic substrate in order to measure the growth of particles and phase transitions of particles as a function of RH as it has been shown before that hydrophobicity/hydrophilicity of the substrate can influence the observed hygroscopicity of inorganic salts and spatial distribution of organic and inorganic phases in mixed substrate deposited particles.[11,39]

Sodium Chloride Mixed with Malonic Acid, 2:1 Molar Ratio. It has been shown previously that in aqueous micrometer size droplets NaCl can react with organic acids through acid displacement reactions releasing gas-phase HCl and forming organic salts in the particle phase according to reaction 1 below.[40]

$$\mathrm{NaCl_{(aq)}} + \mathrm{HA_{(aq)}} \leftrightarrows \mathrm{NaA_{(aq)}} + \mathrm{HCl_{(aq,g)}} \quad (R1)$$

where HA represents atmospherically relevant organic acids.

This reaction may therefore lead to a depletion in the chloride levels in the particle due to the formation of hydrogen chloride gas. However, chloride is not completely depleted for the NaCl/MA mixture used here, and it has been reported using the same conditions that approximately half of the chloride in the particle is removed through reaction 1.[40] This is consistent with our results showing 43% reduction of Cl in the NaCl/MA acid mixture as compared with NaCl using elemental analysis. Thus, the resulting particles are expected to be a mixture of the excess of NaCl and sodium hydrogen malonate rather than pure sodium hydrogen malonate. AFM phase images of sub- and supermicrometer sized particles are shown in Figure 3a. Particles in the submicrometer size range are shown on the right, supermicrometer particles are shown on the left. As can be seen from these images, both, submicrometer and supermicrometer particles are homogeneous, showing a single value for phase as indicated by the uniform color in the image. The SEM/EDX map in Figure 3b shows distribution of Cl, Na, C, and O in a supermicrometer particle. As can be seen from the SEM/EDX data, there is a uniform distribution of all these elements which means that NaCl and sodium hydrogen malonate are distributed homogeneously throughout the particle.

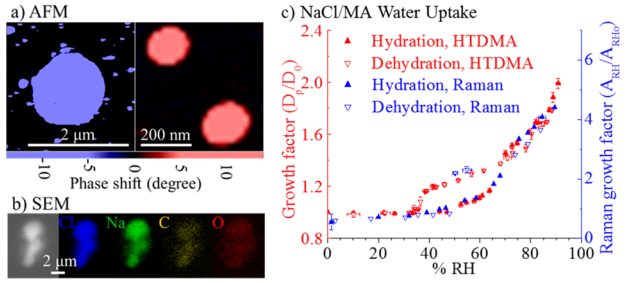

Figure 3. (a) AFM phase images at 10% RH of submicrometer and supermicrometer NaCl/MA (2:1 molar ratio) particles and (b) SEM image and Cl, Na, C, O, elemental maps of a supermicrometer particle captured at 20% RH in a WETSEM capsule; (c) hygroscopicity measured by HTDMA for 100 nm particles (red triangles) and by micro-Raman spectroscopy for supermicrometer particles (blue triangles).

Figure 3c shows hygroscopicity curves of mixed NaCl/MA particles measured by HTDMA (red) and micro-Raman spectroscopy (blue). Determined DRH and ERH values are summarized in Table 1. These particles start to absorb water at approximately 40% and become fully deliquesced at 67.0 ± 4.4% RH (submicrometer) and 71.8 ± 5.3% RH (supermicrometer) which is lower than DRH of NaCl (74−76% RH). It was shown before that NaCl/MA mixed particles start to uptake water at RH values below DRH and fully deliquesce between 50 and 75% RH, while hysteresis between hydration/dehydration cycles diminishes as the ratio between organic and inorganic components increases.[12,41,42] The decrease in DRH values and homogeneous composition of NaCl/MA particles at submicrometer and supermicrometer sizes are also consistent with previous observations that homogeneously mixed inorganic/organic particles decrease the DRH of inorganic components.[3−8]

Ammonium Sulfate Mixed with Adipic Acid, 1:1 Weight Ratio. AFM phase images of sub- and supermicrometer mixed AS/AA particles are shown in Figure 4a; the Raman chemical functional map of a supermicrometer

DOI: 10.1021/jp510268p
J. Phys. Chem. A 2015, 119, 4489−4497

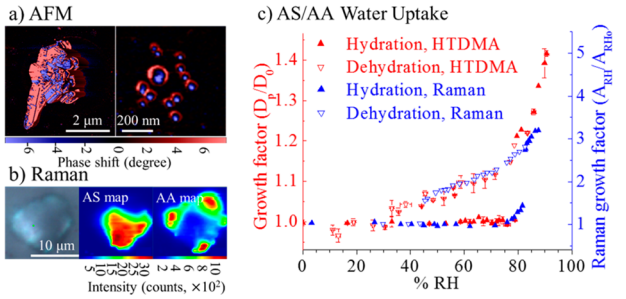

Figure 4. (a) AFM phase images at 10% RH of submicrometer and supermicrometer AS/AA particles and (b) Raman image and AS and AA maps of a supermicrometer particle at 20% RH; (c) hygroscopicity measured by HTDMA for 100 nm particles (red triangles) and micro-Raman spectroscopy for supermicrometer particles (blue triangles).

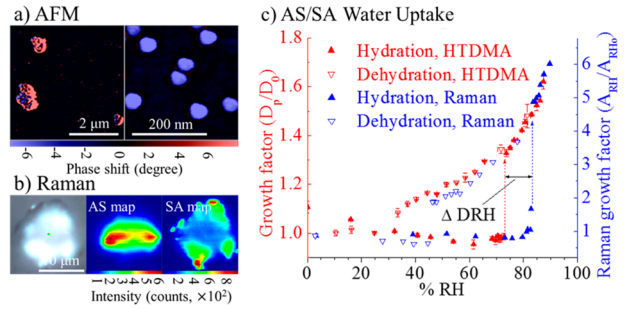

Figure 5. (a) AFM phase images at 10% RH of submicrometer and supermicrometer AS/SA particles and (b) Raman image and AS and SA maps of a supermicrometer particle at 20% RH; (c) hygroscopicity measured by HTDMA for 100 nm particles (red triangles) and micro-Raman spectroscopy for supermicrometer particles (blue triangles). Dashed arrows indicate deliquescence of submicrometer (red) and supermicrometer (blue) particles. ΔDRH = 9.5% is the difference between DRH values of submicrometer and 100 nm particles.

particle is shown in Figure 4b. The AS map was obtained by mapping the intensity of the 960−990 cm^{-1} spectral region. For the AA map the intensity of the 900−930 cm^{-1} spectral region was used. Raman spectra of AS, AA, and AS/AA mixture are shown in Supporting Information, Figure S1. Raman chemical maps were used here instead of SEM/EDX as both AS and SA are Raman active. In the case of the NaCl/MA mixture NaCl is not Raman active, therefore elemental maps were used to show spatial distribution of NaCl/MA mixture components. As can be seen in Figure 4, both AFM phase imaging data and Raman maps clearly show these particles are heterogeneous and undergo phase separation at both size ranges. Figure 4 shows AFM image and Raman map of supermicron AS/SA particle at low RH. These were also taken at 80% RH (not shown) and show that particles retain phase segregation at a relative humidity just below deliquescence. Furthermore, Raman maps illustrate that the particle core consists primarily of AS, surrounded by AA. These current results are consistent with earlier reports that show AS/AA particles phase segregate for all sized particles.[43]

Figure 4c shows hygroscopicity curves of mixed AS/AA particles probed by HTDMA (red) and micro-Raman spectroscopy (blue). DRH and ERH values determined from these experiments are summarized in Table 1. The hygroscopic behavior of submicrometer and supermicrometer particles give DRH values of 79.3 ± 0.5% RH (submicrometer) and 82.2 ± 0.6% RH (supermicrometer), which are close to DRH values of AS. These results are consistent with our observation that AA and AS form heterogeneous particles, and as it is noted previously, DRH and ERH points of heterogeneously mixed organic/inorganic systems are typically similar to the DRH and ERH of the inorganic salt component.[6]

Ammonium Sulfate Mixed with Succinic Acid, 1:1 Weight Ratio. AFM phase images of particles aerosolized from an AS/SA mixture are shown in Figure 5a. Raman image and map of supermicrometer particle are shown in Figure 5b. The AS map was obtained by mapping the intensity of 960−990 cm^{-1} spectral region. For the SA map the intensity of 920−950 cm^{-1} spectral regions was used. Raman spectra of the AS, SA, and AS/SA mixture are shown in Supporting Information, Figure S2. Raman maps of AS and SA do not overlap which indicates that the components in these particles have clearly phase separated. It is consistent with earlier published results of small AS/SA particles having a homogeneous morphology, whereas larger particles phase separate into a partially engulfed morphology due to crystallization of the organic component before crystallization of AS.[43]

Hygroscopicity was measured by HTDMA for 100 nm aerosol particles and by Raman for substrate deposited supermicrometer particles. The results are shown in Figure 5c and tabulated in Table 1. As can be seen supermicrometer particles (blue triangles) deliquesce at 82.7 ± 0.3% RH and effloresce at 45.5 ± 1.1% RH which is close to deliquescence and efflorescence points of AS (82.3 ± 2.5% RH and 43.5 ± 2.1% RH respectively, measured for supermicrometer substrate deposited AS particles by Raman). In contrast 100 nm particles deliquesce at 73.2 ± 0.6% RH and effloresce at 29.2 ± 6.1% RH which is lower than these values for AS (DRH of AS is 80.4 ± 0.6% RH and ERH is 37.7 ± 4.1% RH measured for 100 nm particles by HTDMA). The decrease in DRH values and homogeneous composition of 100 nm AS/SA particles and DRH close to AS DRH of supermicrometer AS/SA particles are consistent with previous observations that homogeneously mixed inorganic/organic particles decrease the DRH of the inorganic component and there is little or no change in the DRH and ERH values from those of the salt component in heterogeneous particles.[3−8]

Marine Chloride Mixture. AFM phase images of particles aerosolized from Na, Mg, K, and Ca chlorides are shown in Figure 6a. Particles in the submicrometer size range are shown on the right, whereas supermicrometer particles are shown on the left. As can be seen from these images, submicrometer particles are homogeneous while supermicrometer particles are not as indicated by the phase image showing very distinct values of the phase shifts. SEM image and SEM/EDX maps of supermicrometer particles captured in the WETSEM capsule at ambient conditions (20% RH) are shown in Figure 6b. Na, Mg, Ca, and K elemental maps clearly do not overlap and show clear evidence for phase separation. AFM image and EDX map of supermicron mixed chloride particle were additionally taken at 70% (not shown). These image and map indeed show phase separation.

Hygroscopicity was measured by HTDMA for 100 nm aerosol particles and by Raman for substrate deposited supermicrometer particles. The results are shown in Figure 6c and tabulated in Table 1. As can be seen supermicrometer particles (blue triangles) deliquesce at 75.3 ± 1.1% RH and effloresce at 49.0 ± 0.7% RH which is close to deliquescence

DOI: 10.1021/jp510268p
J. Phys. Chem. A 2015, 119, 4489−4497

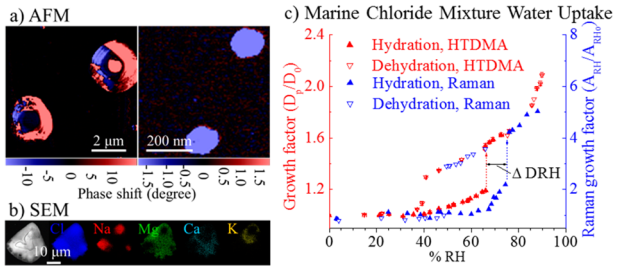

Figure 6. (a) AFM phase images of marine chloride mixture at 10% RH of submicrometer (right) and supermicrometer (left) particles and (b) SEM image and Cl, Na, Mg, Ca, K elemental maps of a supermicrometer particle captured at 20% RH in a WETSEM capsule; (c) hygroscopicity of mixed chloride particles measured by HTDMA for 100 nm particles (red triangles) and micro-Raman spectroscopy for supermicrometer particles (blue triangles). Dashed arrows indicate deliquescence of submicrometer (red) and supermicrometer (blue). ΔDRH = 9.2% is the difference between DRH values of submicrometer and 100 nm particles.

and efflorescence points of NaCl (77.5 ± 2.1% RH and 52.8 ± 1.1% RH, respectively, measured for supermicrometer substrate deposited NaCl particles by Raman). In contrast, 100 nm particles deliquesce at 66.1 ± 0.1 RH and effloresce at 40.0 ± 1.2% RH which is lower of those value for NaCl (DRH of NaCl is 74.0 ± 0.2% RH and 43.0 ± 1.0% RH measured for 100 nm NaCl particles by HTDMA).

DISCUSSION

Multicomponent aerosols have different hygroscopic behaviors depending on whether they are uniformly mixed particles or if they phase separate. This has been well established in the literature.[3−5,7,8] The main differences observed for these different mixing states are as follows. For homogeneous mixtures of organic matter with an inorganic component, the values of both the DRH and ERH are lower relative to the pure inorganic salt. As a result, these particles can remain in the liquid state for a RH range typical in the atmosphere. Other organic molecules tend to phase separate from aqueous inorganic salt causing little to no change in DRH and ERH values.[5] For AS it was shown that the nature of secondary organic material (SOM) determines if DRH and ERH values are equal or lower than that of the pure ammonium sulfate. For example, products of dark ozonolysis of α-pinene do not influence DRH and ERH of ammonium sulfate in mixed particles while SOM produced by photo-oxidation of α-pinene were shown to decrease DRH and ERH of AS particles in mixtures.[3,5] Interestingly, the morphology of phase-separated particles depends on composition, including organic material, inorganic salt, and organic to inorganic ratio.[8] The actual morphology of organic/inorganic mixed particles can be expected to vary with a dependence on the organic volume fraction, the particle size, and the relative surface tensions of the two phases with air as well with each other.[44] AFM image and EDX map of supermicron mixed chloride particle were additionally taken at 70% (not shown). These image and map indeed show phase separation. The phase-separated morphologies of the submicrometer aerosol particles studied by HTDMA could be different from those of supermicrometer supported particles studied in the microscopy experiments.[5] In the supermicrometer mixed polyethylene glycol/AS particles, the number of inorganic inclusions in the organic phase was found to depend on the size of the entire particle. The number of AS satellite inclusions in the outer phase decreases with decreasing size of particles.[45] Highly polar organic substances with high O:C ratios may increase the solubility of AS in the aqueous organic mixtures and thus decrease ERH and DRH of AS. Moreover, high viscosity in organic-rich particles may hinder the crystallization of AS.

SA deliquesces close to 100% RH and has very low solubility in water.[46] Therefore, in AS/SA particles that are phase separated SA acts almost inert during deliquescence of AS. Therefore, the deliquescence and efflorescence of an externally mixed AS/SA particle are controlled by AS, and DRH and ERH values are close to that of AS. This result is consistent with the observations of Choi et al. that were carried out for supermicrometer mixed AS/SA particles.[41]

One of the factors that determine morphologies of mixed organic/inorganic particles is the surface tension. The shape of a droplet composed of two liquid phases can be calculated using the surface tensions of each of the components.[32] On the basis of calculations by Song et al., it was shown that the most favorable configurations of supermicrometer mixed AS/organic particles are core−shell or partially engulfed morphologies with an organic-rich phase being on the outer surface of the AS-rich phase. However, they note that this prediction is only strictly valid for phases of infinite volume where the surface and interfacial area changes can be approximated as being the same. In cases of finite volumes when the spreading coefficient is close to zero, the morphology predictions may become less reliable.[32] The surface tension of aqueous AS solution is 88.8 mN/m at a_w = 0.8 (solution saturation of AS).[47] The surface tension of SA can be calculated from eq 5:[48]

$$\sigma = 83.45 - 0.12T \quad (5)$$

Where T is the temperature in K. At T = 293 K, the surface tension of SA is 48.29 mN/m which is significantly lower than that of the aqueous AS solution. The morphology of a droplet containing two immiscible liquids will adjust to minimize the surface energy that can be achieved when the liquid with lower surface tension is at the surface,[45] so in SA/AS particles, the outer phase is expected to be the SA-rich phase. This result is in fact supported by the Raman maps shown in Figure 5b. However, it can also be seen from the Raman maps that the SA does not completely coat the AS core. Particles composed of an aqueous salt and organic component with limited aqueous solubility preferentially form partially engulfed structures;[49] however, it is also sometimes the result of drying of particles with core−shell morphologies that give this more heterogeneous "patchy" outer coating.[32] Interestingly, a range of partially engulfed structures was observed by Buajarern et al. using the decane/NaCl system that was also shown to depend on relative sizes of organic and aqueous droplets.[50] This result is also supported by observation that in spatially separated organic/inorganic particles the outer phase is predominantly organic.[7]

Phase separation does not occur in smaller particles most likely due to different drying rates as small particles have higher surface to volume ratio, higher evaporation rates, and therefore dry more rapidly. This rapid drying can inhibit partitioning of the AS and SA into two separate phases. Furthermore, the addition of an organic component in small homogeneous particles leads to a decrease in the solution saturation with respect to AS for a constant RH. This leads to a decrease in the DRH to maintain unity saturation; and in a decrease in the ERH to maintain critical supersaturation.[4] It has been shown

DOI: 10.1021/jp510268p
J. Phys. Chem. A 2015, 119, 4489−4497

that for small homogeneous particles dissolution of soluble organic molecules into an aqueous ammonium sulfate phase can inhibit crystallization of the inorganic phase.[51]

The reason that submicrometer AS/SA is homogeneous while AS/AA is phase separated can be attributed to a difference in their solubility. It has been shown that mixed particles contain components with different solubilities for inhomogeneous structures.[52] AS is more soluble than both, SA and AA. Additionally AA has a lower solubility than SA and therefore the AS/AA mixture represents the system with the largest difference in solubility between components and that can be the reason for these mixed particles to phase separate at all sizes.

For mixtures of inorganic salts, theoretical predictions show that the DRH of one electrolyte is lowered by the addition of a second electrolyte.[53] Ge et al. examined the crystallization of droplets of a two-electrolyte system consisting of NaCl/KCl of the different proportions between NaCl and KCl and showed that their hygroscopic behavior as well as composition and homogeneity of the dried particle depends on relative proportions of NaCl and KCl. In solution, where KCl wt % is lower than an eutonic composition, a dried particle is composed of a pure NaCl core surrounded by a coating of eutonic composition.[54] If this dried particle is subjected to an increase in RH, the particle will remain unchanged until mutual DRH (MDRH) is reached (that is lower than DRH of both NaCl and KCl). The coating, having eutonic composition at the particle surface, is then dissolved in the absorbed water layer. Further increasing the RH results in more water absorbed into the particle, and part of the pure NaCl solid core is dissolved to maintain the water equilibrium between the solution and the atmosphere. At a certain RH, which is close to but lower than the DRH of the pure NaCl solid core, there is complete dissolution, and the particle becomes an aqueous droplet. In solution where the KCl wt % is higher than required to form an eutonic composition, a dried particle is composed of a pure KCl core surrounded by a coating of eutonic composition. When a particle of this composition is introduced to increasing RH, it starts to absorb water at MDRH but completely dissolves at the RH between MDRH and KCl DRH. In a solution of eutonic composition the particle crystallizes or deliquesces like pure salt at MDRH. The phase transformation either from aqueous to solid or from solid to aqueous occurs abruptly, and the dried particles of this composition are morphologically and chemically uniform. Additionally, using surface sensitive techniques Ge et al. detected water adsorbed on the particle surface at RH lower than the MDRH.[54] In contrast, it was recently shown that the ERH minimum of mixed supermicrometer NaCl and KCl aerosol particles is different from the theoretically expected MERH at the eutonic mixture. It was suggested that efflorescence is driven by crystallization of a more supersaturated salt and that the degree of KCl and NaCl supersaturation is affected by short-range ionic interactions and common-ion effect.[55]

Hygroscopicity curves for a marine chloride mixture derived from HTDMA and micro-Raman spectroscopy experiments indicate that these particles take up water prior to the deliquescence points due to the presence of Mg and Ca chlorides (DRH = 33 and 29% RH, respectively).[56] Homogeneous particles of 100 nm start to pick up water at approximately 30% RH until they finally deliquesce at 66.1% RH, after which NaCl homogeneously distributed within a particle gradually dissolves in the solution as RH increases. In supermicrometer particles, chlorides are spatially separated with NaCl being the predominant phase as expected given that the relative concentrations of the chloride mixture used here were for seawater. More hygroscopic components (Mg and Ca chlorides) start to absorb water and deliquesce at a RH lower than the deliquescence point of NaCl, causing the gradual slope of the hygroscopicity curve prior to the NaCl DRH. However, as the majority of the particle is NaCl, the complete deliquescence occurs at the DRH of NaCl. It is not clear though why 100 nm particles deliquesce at lower RH and retain water longer than supermicrometer particles.

One additional consideration in this is that the observed difference in mixing state and hygroscopic properties can potentially be due to differences in particle composition due to an inherent fractionation of chemical components upon aerosol formation. It has been shown for atmospheric samples that larger particles are dominated by inorganics, whereas smaller particles are dominated by organics.[57,58] Remarkably, it has been shown that this effect can depend on the aerosol production method. In particular, for sea spray aerosol it has been shown that wavebreaking produces aerosol particles that are enriched with organics in only smaller sizes, whereas aerosol particles produced by forcing air through submerged sintered glass filters are more enriched with organics at all sizes.[59] Therefore, it can be proposed that transfer of the solution components used in this study to the aerosol phase can depend on the size of the particle. Further studies of chemical fractionation are warranted and may play a role in the composition of aerosols. In this case, larger particles might be organic depleted and therefore retain hygroscopicity behavior similar to that of the inorganic component, whereas smaller particles might be organic enriched and show different hygroscopic behavior. However, this hypothesis is not applicable to the observed difference in mixing state and hygroscopicity of inorganic particles formed from a marine chloride mixture. Thus, further investigations need to consider these particles types, that is, mixtures of inorganic components, as well.

CONCLUSIONS

In this study, it has been shown that hygroscopicity measured by methods that use substrate deposited particles (micro-Raman spectroscopy) and substrate free approach (HTDMA) as well as different particles sizes (submicrometer for HTDMA and supermicrometer in micro-Raman spectroscopy) can be both be used to study particle hygroscopicity. Both methods show reliable results that agree well with literature data and theoretical predictions. Using these two methods, size dependent hygroscopicity of variety of atmospheric aerosol mixtures were measured. A number of multicomponent systems were studied here including proxies of SOM (AS with AA and SA) and proxies of sea spray aerosol particles (mixture of Na, Mg, K and Ca chlorides as well as NaCl mixed with MA). Particle heterogeneity was determined using AFM, Raman maps and SEM/EDX maps. Our results show that hygroscopicity behavior of some of these mixed particles depends on their size. Interestingly, it was determined that particles composed of AS with SA and of marine chloride mixtures typical for marine environment show different hygroscopicity behavior at different sizes that can be related to differences in morphology.

Very often studies of hygroscopicity of atmospherically relevant particles are performed on supermicrometer particles. However, as shown here, hygroscopicity for some particles

DOI: 10.1021/jp510268p
J. Phys. Chem. A 2015, 119, 4489−4497

depend on particle size. Smaller particles in accumulation mode are more typical for long-range transported aerosols. For systems studied here that show size-dependent hygroscopicity behavior submicrometer particles have lower deliquescence and efflorescence RH values then larger particles. Adsorbed water plays an important role in the reaction chemistry and therefore revealed that morphology-dependent hygroscopicity has consequences for heterogeneous atmospheric chemistry as well as for scattering and absorbing solar radiation, and cloud condensation nuclei activity. These results help us better understand the role of aerosol particles in heterogeneous atmospheric chemistry and the Earth's climate system.

■ ASSOCIATED CONTENT

Supporting Information

Figure S1. Raman spectra of AS and AA particles (black) and AS/AA mixed particles (red). Blue box highlights the region used to construct an AA map (900−930 cm^{-1}), red box highlights the region used to construct an AS map (960−990 cm^{-1}). Figure S2. Raman spectra of AS and SA particles (black) and AS/SA mixed particles (red). Blue box highlights the region used to construct a SA map (920−950 cm^{-1}), red box highlights the region used to construct an AS map (960−990 cm^{-1}). This material is available free of charge via the Internet at http://pubs.acs.org.

■ AUTHOR INFORMATION

Corresponding Authors

*E-mail: alexei-tivanski@uiowa.edu.
*E-mail: vicki-grassian@uiowa.edu.

Notes

The authors declare no competing financial interest.

■ ACKNOWLEDGMENTS

We thank Professor Miriam A. Freedman for helpful discussions. This work was funded by the National Science Foundation through the Center for Aerosol Impacts on Climate and the Environment under Grant No. CHE 1305427. Any opinions, findings, and conclusions or recommendations expressed in this material are those of the authors and do not necessarily reflect the views of the National Science Foundation.

■ REFERENCES

(1) Collins, D. B.; Ault, A. P.; Moffet, R. C.; Ruppel, M. J.; Cuadra-Rodriguez, L. A.; Guasco, T. L.; Corrigan, C. E.; Pedler, B. E.; Azam, F.; Aluwihare, L. I.; et al. Impact of Marine Biogeochemistry on the Chemical Mixing State and Cloud Forming Ability of Nascent Sea Spray Aerosol. *J. Geophys. Res.-Atmos.* **2013**, *118*, 8553−8565.

(2) Burrows, S. M.; Ogunro, O.; Frossard, A. A.; Russell, L. M.; Rasch, P. J.; Elliott, S. A Physically-Based Framework for Modelling the Organic Fractionation of Sea Spray Aerosol from Bubble Film Langmuir Equilibria. *Atmos. Chem. Phys. Discuss.* **2014**, *14*, 5375−5443.

(3) Smith, M. L.; Bertram, A. K.; Martin, S. T. Deliquescence, Efflorescence, and Phase Miscibility of Mixed Particles of Ammonium Sulfate and Isoprene-Derived Secondary Organic Material. *Atmos. Chem. Phys.* **2012**, *12*, 9613−9628.

(4) Bertram, A. K.; Martin, S. T.; Hanna, S. J.; Smith, M. L.; Bodsworth, A.; Chen, Q.; Kuwata, M.; Liu, A.; You, Y.; Zorn, S. R. Predicting the Relative Humidities of Liquid−Liquid Phase Separation, Efflorescence, and Deliquescence of Mixed Particles of Ammonium Sulfate, Organic Material, and Water Using the Organic-to-Sulfate Mass Ratio of the Particle and the Oxygen-to-Carbon Elemental Ratio of the Organic Component. *Atmos. Chem. Phys.* **2011**, *11*, 10995−11006.

(5) Smith, M. L.; You, Y.; Kuwata, M.; Bertram, A. K.; Martin, S. T. Phase Transitions and Phase Miscibility of Mixed Particles of Ammonium Sulfate, Toluene-Derived Secondary Organic Material, and Water. *J. Phys. Chem. A* **2013**, *117*, 8895−8906.

(6) Smith, M. L.; Kuwata, M.; Martin, S. T. Secondary Organic Material Produced by the Dark Ozonolysis of α-Pinene Minimally Affects the Deliquescence and Efflorescence of Ammonium Sulfate. *Aerosol Sci. Technol.* **2011**, *45*, 244−261.

(7) Peckhaus, A.; Grass, S.; Treuel, L.; Zellner, R. Deliquescence and Efflorescence Behavior of Ternary Inorganic/Organic/Water Aerosol Particles. *J. Phys. Chem. A* **2012**, *116*, 6199−6210.

(8) You, Y.; Smith, M. L.; Song, M.; Martin, S. T.; Bertram, A. K. Liquid−Liquid Phase Separation in Atmospherically Relevant Particles Consisting of Organic Species and Inorganic Salts. *Int. Rev. Phys. Chem.* **2014**, *33*, 43−77.

(9) Veghte, D. P.; Altaf, M. B.; Freedman, M. A. Size Dependence of the Structure of Organic Aerosol. *J. Am. Chem. Soc.* **2013**, *135*, 16046−16049.

(10) Gysel, M.; Weingartner, E.; Baltensperger, U. Hygroscopicity of Aerosol Particles at Low Temperatures. 2. Theoretical and Experimental Hygroscopic Properties of Laboratory Generated Aerosols. *Environ. Sci. Technol.* **2002**, *36*, 63−68.

(11) Zhou, Q.; Pang, S.-F.; Wang, Y.; Ma, J.-B.; Zhang, Y.-H. Confocal Raman Studies of the Evolution of the Physical State of Mixed Phthalic Acid/Ammonium Sulfate Aerosol Droplets and the Effect of Substrates. *J. Phys. Chem. B* **2014**, *118*, 6198−6205.

(12) Ma, Q.; Ma, J.; Liu, C.; Lai, C.; He, H. Laboratory Study on the Hygroscopic Behavior of External and Internal C2−C4 Dicarboxylic Acid−NaCl Mixtures. *Environ. Sci. Technol.* **2013**, *47*, 10381−10388.

(13) Duplissy, J.; Gysel, M.; Sjogren, S.; Meyer, N.; Good, N.; Kammermann, L.; Michaud, V.; Weigel, R.; Martins dos Santos, S.; Gruening, C.; et al. Intercomparison Study of Six HTDMAS: Results and Recommendations. *Atmos. Meas. Technol.* **2009**, *2*, 363−378.

(14) Koehler, K. A.; Kreidenweis, S. M.; DeMott, P. J.; Prenni, A. J.; Carrico, C. M.; Ervens, B.; Feingold, G. Water Activity and Activation Diameters from Hygroscopicity Data - Part II: Application to Organic Species. *Atmos. Chem. Phys.* **2006**, *6*, 795−809.

(15) Krieger, U. K.; Marcolli, C.; Reid, J. P. Exploring the Complexity of Aerosol Particle Properties and Processes Using Single Particle Techniques. *Chem. Soc. Rev.* **2012**, *41*, 6631−6662.

(16) Lee, A. K. Y.; Ling, T. Y.; Chan, C. K. Understanding Hygroscopic Growth and Phase Transformation of Aerosols Using Single Particle Raman Spectroscopy in an Electrodynamic Balance. *Faraday Discuss.* **2008**, *137*, 245−263.

(17) Holland, H. D. *The Chemistry of the Atmosphere and Oceans*; Wiley: New York, 1978.

(18) Kawamura, K.; Umemoto, N.; Mochida, M.; Bertram, T.; Howell, S.; Huebert, B. J. Water-Soluble Dicarboxylic Acids in the Tropospheric Aerosols Collected over East Asia and Western North Pacific by Ace-Asia C-130 Aircraft. *J. Geophys. Res.: Atmos.* **2003**, *108*, 8639.

(19) Chen, Q.; Farmer, D. K.; Schneider, J.; Zorn, S. R.; Heald, C. L.; Karl, T. G.; Guenther, A.; Allan, J. D.; Robinson, N.; Coe, H.; et al. Mass Spectral Characterization of Submicrometer Biogenic Organic Particles in the Amazon Basin. *Geophys. Res. Lett.* **2009**, *36*, L20806.

(20) Zhang, Q.; Jimenez, J. L.; Canagaratna, M. R.; Allan, J. D.; Coe, H.; Ulbrich, I.; Alfarra, M. R.; Takami, A.; Middlebrook, A. M.; Sun, Y. L.; et al. Ubiquity and Dominance of Oxygenated Species in Organic Aerosols in Anthropogenically-Influenced Northern Hemisphere Midlatitudes. *Geophys. Res. Lett.* **2007**, *34*, L13801.

(21) Jimenez, J. L.; Canagaratna, M. R.; Donahue, N. M.; Prevot, A. S. H.; Zhang, Q.; Kroll, J. H.; DeCarlo, P. F.; Allan, J. D.; Coe, H.; Ng, N. L.; et al. Evolution of Organic Aerosols in the Atmosphere. *Science* **2009**, *326*, 1525−1529.

(22) Baustian, K. J.; Wise, M. E.; Tolbert, M. A. Depositional Ice Nucleation on Solid Ammonium Sulfate and Glutaric Acid Particles. *Atmos. Chem. Phys.* **2010**, *10*, 2307−2317.

DOI: 10.1021/jp510268p
J. Phys. Chem. A 2015, 119, 4489−4497

(23) Dong, J.-L.; Li, X.-H.; Zhao, L.-J.; Xiao, H.-S.; Wang, F.; Guo, X.; Zhang, Y.-H. Raman Observation of the Interactions between NH_4^+, SO_4^{2-}, and H_2O in Supersaturated $(NH_4)_2SO_4$ Droplets. *J. Phys. Chem. B* **2007**, *111*, 12170−12176.
(24) Spinner, E. Raman-Spectral Depolarisation Ratios of Ions in Concentrated Aqueous Solution. The Next-to-Negligible Effect of Highly Asymmetric Ion Surroundings on the Symmetry Properties of Polarisability Changes During Vibrations of Symmetric Ions. Ammonium Sulphate and Tetramethylammonium Bromide. *Spectrochim. Acta, Part A* **2003**, *59*, 1441−1456.
(25) Baltrusaitis, J.; Grassian, V. H. Calcite Surface in Humid Environments. *Surf. Sci.* **2009**, *603*, L99−L104.
(26) García, R.; Pérez, R. Dynamic Atomic Force Microscopy Methods. *Surf. Sci. Rep.* **2002**, *47*, 197−301.
(27) Schuttlefield, J.; Al-Hosney, H.; Zachariah, A.; Grassian, V. H. Attenuated Total Reflection Fourier Transform Infrared Spectroscopy To Investigate Water Uptake and Phase Transitions in Atmospherically Relevant Particles. *Appl. Spectrosc.* **2007**, *61*, 283−292.
(28) Han, J. H.; Martin, S. T. Heterogeneous Nucleation of the Efflorescence of $(NH_4)_2SO_4$ Particles Internally Mixed with Al_2O_3, TiO_2, and ZrO_2. *J. Geophys. Res.-Atmos.* **1999**, *104*, 3543−3553.
(29) Cziczo, D. J.; Nowak, J. B.; Hu, J. H.; Abbatt, J. P. D. Infrared Spectroscopy of Model Tropospheric Aerosols as a Function of Relative Humidity: Observation of Deliquescence and Crystallization. *J. Geophys. Res.-Atmos* **1997**, *102*, 18843−18850.
(30) Dougle, P. G.; Veefkind, J. P.; ten Brink, H. M. Crystallisation of Mixtures of Ammonium Nitrate, Ammonium Sulphate and Soot. *J. Aerosol Sci.* **1998**, *29*, 375−386.
(31) Tang, I. N.; Munkelwitz, H. R. Water Activities, Densities, and Refractive Indices of Aqueous Sulfates and Sodium Nitrate Droplets of Atmospheric Importance. *J. Geophys. Res.-Atmos.* **1994**, *99*, 18801−18808.
(32) Song, M. J.; Marcolli, C.; Krieger, U. K.; Lienhard, D. M.; Peter, T. Morphologies of Mixed Organic/Inorganic/Aqueous Aerosol Droplets. *Faraday Discuss.* **2013**, *165*, 289−316.
(33) Tang, I. N.; Munkelwitz, H. R. Phase-Transformation and Droplet Growth of Sulfate Aerosols. *Abstr. Pap. Am. Chem. S.* **1977**, *173*, 60.
(34) Wise, M. E.; Semeniuk, T. A.; Bruintjes, R.; Martin, S. T.; Russell, L. M.; Buseck, P. R. Hygroscopic Behavior of NaCl-Bearing Natural Aerosol Particles Using Environmental Transmission Electron Microscopy. *J. Geophys. Res.-Atmos.* **2007**, *112*, 12.
(35) Weis, D. D.; Ewing, G. E. Water Content and Morphology of Sodium Chloride Aerosol Particles. *J. Geophys. Res.-Atmos.* **1999**, *104*, 21275−21285.
(36) Kohler, H. The Nucleus in and the Growth of Hygroscopic Droplets. *Trans. Faraday Soc.* **1936**, *32*, 1152−1161.
(37) Kreidenweis, S. M.; Koehler, K.; DeMott, P. J.; Prenni, A. J.; Carrico, C.; Ervens, B. Water Activity and Activation Diameters from Hygroscopicity Data—Part I: Theory and Application to Inorganic Salts. *Atmos. Chem. Phys.* **2005**, *5*, 1357−1370.
(38) Gibson, E. R.; Hudson, P. K.; Grassian, V. H. Physicochemical Properties of Nitrate Aerosols: Implications for the Atmosphere. *J. Phys. Chem. A* **2006**, *110*, 11785−11799.
(39) Eom, H.-J.; Gupta, D.; Li, X.; Jung, H.-J.; Kim, H.; Ro, C.-U. Influence of Collecting Substrates on the Characterization of Hygroscopic Properties of Inorganic Aerosol Particles. *Anal. Chem.* **2014**, *86*, 2648−2656.
(40) Laskin, A.; Moffet, R. C.; Gilles, M. K.; Fast, J. D.; Zaveri, R. A.; Wang, B.; Nigge, P.; Shutthanandan, J. Tropospheric Chemistry of Internally Mixed Sea Salt and Organic Particles: Surprising Reactivity of NaCl with Weak Organic Acids. *J. Geophys. Res.-Atmos.* **2012**, *117*, D15302.
(41) Choi, M. Y.; Chan, C. K. The Effects of Organic Species on the Hygroscopic Behaviors of Inorganic Aerosols. *Environ. Sci. Technol.* **2002**, *36*, 2422−2428.
(42) Ghorai, S.; Wang, B.; Tivanski, A.; Laskin, A. Hygroscopic Properties of Internally Mixed Particles Composed of NaCl and Water-Soluble Organic Acids. *Environ. Sci. Technol.* **2014**, *48*, 2234−2241.
(43) Veghte, D. P.; Bittner, D. R.; Freedman, M. A. Cryo-transmission Electron Microscopy Imaging of the Morphology of Submicrometer Aerosol Containing Organic Acids and Ammonium Sulfate. *Anal. Chem.* **2014**, *86*, 2436−2442.
(44) Kwamena, N. O. A.; Buajarern, J.; Reid, J. P. Equilibrium Morphology of Mixed Organic/Inorganic/Aqueous Aerosol Droplets: Investigating the Effect of Relative Humidity and Surfactants. *J. Phys. Chem. A* **2010**, *114*, 5787−5795.
(45) Ciobanu, V. G.; Marcolli, C.; Krieger, U. K.; Weers, U.; Peter, T. Liquid−Liquid Phase Separation in Mixed Organic/Inorganic Aerosol Particles. *J. Phys. Chem. A* **2009**, *113*, 10966−10978.
(46) Parsons, M. T.; Mak, J.; Lipetz, S. R.; Bertram, A. K. Deliquescence of Malonic, Succinic, Glutaric, and Adipic Acid Particles. *J. Geophys. Res.-Atmos.* **2004**, *109*, D06212.
(47) Lewis, E. R. The Effect of Surface Tension (Kelvin Effect) on the Equilibrium Radius of a Hygroscopic Aqueous Aerosol Particle. *J. Aerosol Sci.* **2006**, *37*, 1605−1617.
(48) Hyvärinen, A.-P.; Lihavainen, H.; Gaman, A.; Vairila, L.; Ojala, H.; Kulmala, M.; Viisanen, Y. Surface Tensions and Densities of Oxalic, Malonic, Succinic, Maleic, Malic, and Cis-pinonic Acids. *J. Chem. Eng. Data* **2005**, *51*, 255−260.
(49) Reid, J. P.; Dennis-Smither, B. J.; Kwamena, N.-O. A.; Miles, R. E. H.; Hanford, K. L.; Homer, C. J. The Morphology of Aerosol Particles Consisting of Hydrophobic and Hydrophilic Phases: Hydrocarbons, Alcohols and Fatty Acids as the Hydrophobic Component. *Phys. Chem. Chem. Phys.* **2011**, *13*, 15559−15572.
(50) Buajarern, J.; Mitchem, L.; Reid, J. P. Characterizing Multiphase Organic/Inorganic/Aqueous Aerosol Droplets. *J. Phys. Chem. A* **2007**, *111*, 9054−9061.
(51) Moore, R. H.; Raymond, T. M. HTDMA Analysis of Multicomponent Dicarboxylic Acid Aerosols with Comparison to UNIFAC and ZSR. *J. Geophys. Res.-Atmos.* **2008**, *113*, D04206.
(52) Freney, E. J.; Adachi, K.; Buseck, P. R. Internally Mixed Atmospheric Aerosol Particles: Hygroscopic Growth and Light Scattering. *J. Geophys. Res.-Atmos.* **2010**, *115*, D19210.
(53) Wexler, A. S.; Seinfeld, J. H. 2nd-Generation Inorganic Aerosol Model. *Atmos. Environ.* **1991**, *25*, 2731−2748.
(54) Ge, Z.; Wexler, A. S.; Johnston, M. V. Deliquescence Behavior of Multicomponent Aerosols. *J. Phys. Chem. A* **1998**, *102*, 173−180.
(55) Li, X.; Gupta, D.; Eom, H.-J.; Kim, H.; Ro, C.-U. Deliquescence and Efflorescence Behavior of Individual NaCl and KCl Mixture Aerosol Particles. *Atmos. Environ.* **2014**, *82*, 36−43.
(56) Park, K.; Kim, J.-S.; Miller, A. A Study on Effects of Size and Structure on Hygroscopicity of Nanoparticles Using a Tandem Differential Mobility Analyzer and TEM. *J. Nanopart. Res.* **2009**, *11*, 175−183.
(57) Facchini, M. C.; Rinaldi, M.; Decesari, S.; Carbone, C.; Finessi, E.; Mircea, M.; Fuzzi, S.; Ceburnis, D.; Flanagan, R.; Nilsson, E. D.; et al. Primary Submicrometer Marine Aerosol Dominated by Insoluble Organic Colloids and Aggregates. *Geophys. Res. Lett.* **2008**, *35*, L17814.
(58) Prather, K. A.; Bertram, T. H.; Grassian, V. H.; Deane, G. B.; Stokes, M. D.; DeMott, P. J.; Aluwihare, L. I.; Palenik, B. P.; Azam, F.; Seinfeld, J. H.; et al. Bringing the Ocean into the Laboratory to Probe the Chemical Complexity of Sea Spray Aerosol. *Proc. Natl. Acad. Sci. U.S.A.* **2013**, *110*, 7550−7555.
(59) Collins, D. B.; Zhao, D. F.; Ruppel, M. J.; Laskina, O.; Grandquist, J. R.; Modini, R. L.; Stokes, M. D.; Russell, L. M.; Bertram, T. H.; Grassian, V. H.; et al. Direct Aerosol Chemical Composition Measurements to Evaluate the Physicochemical Differences between Controlled Sea Spray Aerosol Generation Schemes. *Atmos. Meas. Technol. Discuss.* **2014**, *7*, 6457−6499.

DOI: 10.1021/jp510268p
J. Phys. Chem. A 2015, 119, 4489−4497